JACS
JOURNAL OF THE AMERICAN CHEMICAL SOCIETY

ARTICLE

pubs.acs.org/JACS

Remarkable Birefringence in a TiO_2−SiO_2 Composite Film with an Aligned Mesoporous Structure

Hirokatsu Miyata,*[,†] Yuta Fukushima,[‡] Kohei Okamoto,[†] Masahiko Takahashi,[†] Masatoshi Watanabe,[§] Wataru Kubo,[†] Atsushi Komoto,[†] Shin Kitamura,[†] Yosuke Kanno,[‡] and Kazuyuki Kuroda*[,‡,⊥]

[†]Frontier Research Center, Canon Inc., 3-30-2 Shimomaruko, Ohta-ku, Tokyo 146-8501, Japan

[‡]Department of Applied Chemistry, Waseda University, 3-4-1 Ohkubo, Shinjuku-ku, Tokyo 169-8555, Japan

[§]Nanomaterials Technology Development Center, Canon Inc., 3-30-2 Shimomaruko, Ohta-ku, Tokyo 146-8501, Japan

[⊥]Kagami Memorial Research Institute for Materials Science & Technology, Waseda University, 2-8-26 Nishiwaseda, Shinjuku-ku, Tokyo 169-0051 Japan

Supporting Information

ABSTRACT: Mesoporous titania−silica composite films with highly aligned cylindrical pores are prepared by the sol−gel method using a substrate with structural anisotropy. The strong alignment effect of a rubbing-treated polyimide film on a substrate provides a narrow alignment distribution in the plane of the film regardless of the fast condensation rate of titania precursors. The collapse of the mesostructure upon the surfactant removal is effectively suppressed by the reinforcement of the pore walls with silica by exposing the as-deposited film to a vapor of a silicon alkoxide. The existence of a silica layer on the titania pore wall is proved from the distributions of Ti and Si estimated by the elemental analysis in high resolution electron microscopy. The obtained mesoporous titania−silica composite film exhibits a remarkable birefringence reflecting the highly anisotropic mesoporous structure and the high refractive index of titania that forms the pore wall. The Δn value estimated from the optical retardation and the film thickness is larger than 0.06, which cannot be achieved with the conventional mesoporous silica films with uniaxially aligned mesoporous structure even though the alignment of the pores in the films is perfect. These inorganic films with mesoscopic structural anisotropy will find many applications in the field of optics as phase plates with high thermal/chemical/mechanical stabilities.

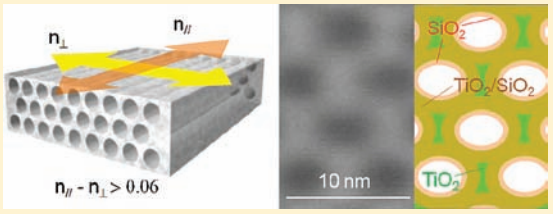

INTRODUCTION

Materials with anisotropic refractive index, birefringence,[1−3] are widely applied in optical devices such as liquid crystal displays, light modulators, and tunable lasers. Films of birefringent materials are especially important as phase plates, which can control the polarization state of light. Usually, phase plates are made of anisotropic organic materials such as uniaxially stretched polycarbonate. However, for some applications, which require high temperature, high photon flux density, and harsh environment, phase plates consisting of stable inorganic materials are desired, and we need to explore such materials that can be formed as a transparent film with a macroscopic structural anisotropy through a simple procedure.

Mesostructured materials with uniform cylindrical mesochannels, prepared through self-assembly of amphiphilic molecules, are promising candidates, which satisfy the above criteria.[4−13] However, the cylindrical mesochannels have to be aligned in one direction in the plane of the films, otherwise the films become macroscopically isotropic regardless of the highly anisotropic shape of the mesochannels. Such mesostructured films with uniaxially oriented channel structure[14−19] have a large structural anisotropy, which can result in optical birefringence. For the practical application as phase plates, the mesostructured films need to have a large anisotropy of refractive index, that is, the Δn value (difference of refractive index for ordinary and extraordinary lights) needs to be large. We have reported the preparation of mesoporous silica films with a highly aligned mesoporous structure on a glass substrate using an anisotropic polymer coating,[14] but the Δn values have not been high enough. We found by calculation that the Δn value of the aligned mesoporous films is largely dependent on the refractive index of the material forming the pore wall and concluded that the large Δn value cannot be achieved as long as we use SiO_2 because of its low refractive index. Use of transparent nonsiliceous materials with a high refractive index, such as TiO_2,[20−31] as a pore wall is indispensable to achieve a large Δn. However, the removal of the template without losing the structural regularity has been difficult to achieve for the nonsiliceous mesostructured materials, especially those with cylindrical mesochannels, and reinforcement of the structure before the removal process has been proposed to prevent the mesostructure from collapsing.[32−36]

Here, we report the successful preparation of a mesoporous titania−silica composite film with a uniaxially oriented porous

Received: May 12, 2011
Published: July 14, 2011

structure which shows a remarkable birefringence with a Δn value larger than 0.06. We control the in-plane orientation of the mesochannels using a rubbing-treated polyimide as an alignment-controlling layer, and the retention of the structure after the template removal is achieved by a vapor treatment of tetramethoxysilane (TMOS) before the calcination process. The obtained film has a good optical quality with high transparency, which enables practical applications. The method in this paper could be applied for the preparation of aligned mesoporous films with various compositions, which would expand the application of these anisotropic mesoporous films.

EXPERIMENTAL SECTION

Preparation of Mesoporous Titania-Silica Composite Films. The details of the preparation of the substrate coated with a rubbing-treated poly(hexamethylenepyromellitimide) are shown in our previous paper.[15] The substrate was spin-coated with a precursor solution prepared by mixing titanium tetraisopropoxide, 1-butanol, Brij56 (nonionic surfactant), hydrochloric acid, and water with the molar ratio of 1.0:29.4:0.15:1.48:5.57 at a speed of 2000 rpm for 20 s. The atmosphere during the spin-coating was controlled to be 25 °C and 60%RH. The film was kept for 1 h in the same atmosphere and then transferred to a 70 mL autoclave containing 3.0 mL of TMOS and sealed at 50 °C for 3 h. The film was taken out from the vessel and was calcined in an air atmosphere at 350 °C for 4 h for the removal of the surfactant.

Characterization. The X-ray diffraction (XRD) profiles with Bragg−Brentano geometry were recorded with a MAC Science M03XHP22 diffractometer using Mn-filtered Fe Kα radiation under the operating conditions of 40 kV and 20 mA. The in-plane XRD was conducted with a Rigaku ATX-G diffractometer equipped with a four-axes goniometer using Cu Kα radiation (50 kV to 300 mA) at a grazing incidence of 0.2°. The details of the in-plane XRD are shown in our previous paper.[15] The morphologies of the cross-section and the surface of the films were characterized using a Hitachi S-5500 high-resolution scanning electron microscope (HR-SEM) at a low accelerating voltage of 2.0−2.5 kV. Cross-sectional images of scanning transmission electron microscopy (STEM) were recorded on a Tecnai F30 at an accelerating voltage of 300 kV in a high angle annular dark field (HAADF) mode, and the distributions of Ti and Si in the images were recorded by energy-dispersive X-ray spectroscopy (EDX) using a silicon solid-state detector.

Optical Measurements. The sample films were placed between the crossed polarizers, and the transmittance of the light from a halogen lamp collimated using a collimating lens was measured with changing the rotation angle ω, which is defined as the angle between the mesochannel direction and the polarization axis of the first polarizer. The transmission $I(\omega)$ was measured with a charge-coupled device (CCD) equipped with a monochromator. The optical retardation R was calculated using eq 1 from the transmittance T and ω. Here, I_0 is the intensity of transmitted light when the sample is placed between the two parallel polarizers with the channel direction parallel to the polarization axis, and λ is the wavelength, 550 nm. The degree of birefringence, the Δn value, was estimated by dividing the obtained retardation value by the thickness of the film, t (eq 2), which was estimated from the cross-sectional SEM images by averaging the thickness of the randomly selected seven points.

$$T = I(\omega)/I_0 = \sin^2(2\omega)\sin^2(\pi R/\lambda) \quad (1)$$

$$\Delta n = R/t \quad (2)$$

Calculation of Δn of an Aligned Mesoporous Film. The structure of a mesoporous film was assumed as follows: two-dimensional hexagonal structure with uniaxial in-plane alignment of cylindrical pores, 150 repeating units in thickness, 4.3 nm periodicity in the ⟨01⟩ direction,

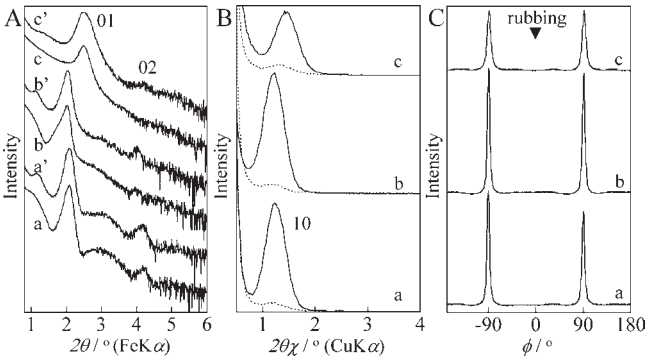

Figure 1. XRD patterns of the mesostructured titania films: (A) $\theta-2\theta$ scanning under the Bragg−Brentano geometry, (B) $\phi-2\theta\chi$ scanning, and (C) ϕ scanning under the in-plane geometry. Traces a, a′ in panel A, a in panels B and C: as-deposited film; b, b′ in panel A, b in panels B and C: after the TMOS vapor treatment; c, c′ in panel A, c in panels B and C: after calcination. Traces a, b, c and a′, b′, c′ in panel A are recorded with the projection of the incident X-rays parallel and perpendicular to the rubbing direction, respectively. Solid lines and dotted lines in panel B are recorded with the projection of the incident X-rays perpendicular and parallel to the rubbing direction at $\phi = 0°$, respectively.

and a 2.0 nm thick pore wall with a refractive index of n. The transmittance of the film with this structure was numerically calculated by a transfer matrix method for the wavelength (λ) from 500 to 700 nm with an interval of 10 nm for the incident lights with parallel and perpendicular polarizations to the aligned pores. The obtained $\lambda-T$ curve was fitted to the theoretical one obtained based on eq 3, which describes the transmission of light in a uniform refractive index of $\tilde{n}$. Here, T_0 is the transmittance at the surface of the film. The Δn was estimated as the difference of the $\tilde{n}$ values obtained for the two polarizations.

$$T = T_0^2/\{T_0^2 + 4(1 - T_0)\sin^2(2\pi\tilde{n}t/\lambda)\} \quad (3)$$

RESULTS AND DISCUSSION

Characterization of the Mesostructured Titania Films. The uniaxial alignment control of mesochannels is achieved by a simple sol−gel method using a rubbing-treated polyimide film. However, the conditions of the coating and the composition of the precursor solution need to be carefully optimized. Especially, control of humidity is very important to achieve the narrow alignment distribution in addition to the high structural regularity. n-Butanol is used to retard the evaporation process to provide enough time for the alignment of the LC phase consisting of cylindrical micelles, and it tends to give a narrower distribution of the in-plane alignment of the mesochannels compared to ethanol.

The XRD patterns of the as-deposited film recorded under the Bragg−Brentano geometry are shown in Figure 1A (traces a and a′). A strong diffraction peak assigned as (01) is observed at a position corresponding to the lattice distance of 5.3 nm. The diffraction intensity is shown on a log scale to display all the diffraction peaks with different intensities simultaneously. The anisotropy caused by the aligned mesostructure is clearly observed, as reported for the aligned mesoporous silica films in our previous paper.[15] The structural anisotropy in the plane of the film is clearly shown by in-plane XRD, as shown in Figure 1B (trace a). The strong in-plane diffraction is observed when the rubbing direction is perpendicular to the projection of the

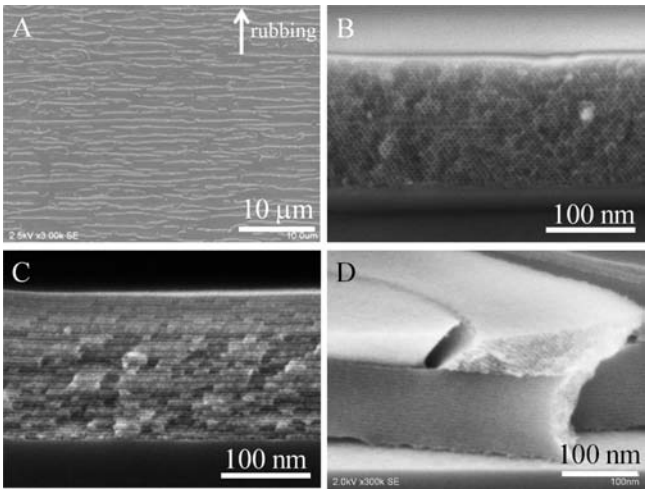

Figure 2. SEM images of the mesoporous titania−silica composite film: low magnification image of the surface (A), high magnification images of the cross-sections cut parallel (B) and perpendicular (C) to the rubbing direction, high magnification image of the parts with a top layer without a controlled alignment (D). The arrow in panel A shows the rubbing direction of polyimide.

incident X-rays. The distribution of the in-plane alignment direction can quantitatively be evaluated by the in-plane XRD rocking curve (Figure 1C trace a). The full width at half-maximum of the in-plane rocking curve is less than 7°, which proves the strict alignment of the mesochannels perpendicular to the rubbing direction. However, the mesochannels need to be hollow to achieve the large Δn value. To prevent the collapse of the regular porous structure, we reinforced the pore wall with silica by exposing this film to a TMOS vapor at 50 °C. The structure of the film scarcely changes by this treatment as confirmed by XRD (Figure 1A traces b, b′, Figure 1B trace b, Figure 1C trace b), except for the small increase of the lattice distance of (01) to 5.5 nm. Deposition of silica on the film surface is not observed by SEM, suggesting that TMOS penetrates into the mesochannels of the mesostructured titania film even before the surfactant removal, which results in the observed slight increase of the lattice distance. By this reinforcement with silica, the aligned mesostructure can be retained after the surfactant removal by calcination at 350 °C, as shown in Figure 1A (traces c and c′), allowing the formation of a mesoporous titania−silica composite film. The complete removal of the surfactant is confirmed by infrared (IR) spectroscopy (Figure S1, Supporting Information). However, the broadening of the diffraction peak and the shift to higher angles shows the contraction of the structure along the thickness direction. The distance of the (01) lattice planes after the surfactant removal is estimated to be 4.5 nm. The in-plane diffraction peak assigned as (10) also shifts to higher angles (Figure 1B trace c), suggesting that the contraction takes place also in the in-plane direction. This contraction causes tiny cracks as small as ∼100 nm, which does not seriously deteriorate the optical performance of the film. The observed structural contraction in the plane of the film as well as the crack formation suggests the weaker adhesion of this mesoporous titania−silica composite film to the substrate compared to that of the aligned mesoporous silica film, which causes neither in-plane contraction nor crack formation. The cracks have a slit-like shape and are aligned parallel to the alignment direction of the mesopores, as shown in Figure 2A.

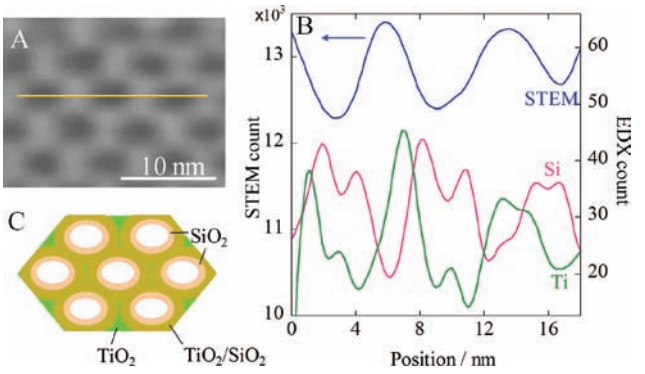

Figure 3. Characterizations of the mesoporous titania−silica composite film with cross-sectional STEM: (A) cross-sectional STEM image, (B) comparison of the line profiles of the STEM image contrast and distributions of Si and Ti, (C) model of the cross-section. The line profiles are obtained along the yellow line shown in panel A.

The film, after the surfactant removal, is extensively characterized by high resolution SEM, and the images are shown in Figure 2B−D. The images of the cross-sections parallel and perpendicular to the rubbing direction are shown in Figure 2B and 2C, respectively. These images clearly show that the alignment is achieved over the whole film thickness of ∼200 nm. The alignment of the pores perpendicular to the rubbing direction is confirmed also by the top-view SEM images (Figure S2A, Supporting Information). In the low-magnification SEM image, Figure 2A, some parts with a curved feature are recognized, which suggests a small coexistence of uncontrolled alignment of the mesopores. Actually, the high resolution SEM images of the surface of those parts reveal the lack of the preferred alignment (Figure S2B, Supporting Information). However, we found that the alignment of the mesopores is partially achieved even in such parts. The representative cross-sectional SEM image of such an area with a curved surface feature is shown in Figure 2D. It is clearly shown that some parts of the film, especially those with the curved surface features, consist of two layers: the bottom layer on the substrate side with a highly aligned mesoporous structure and the top layer beneath the film surface with a random in-plane alignment of the mesopores. This has not been observed in the aligned mesoporous silica film prepared by a sol−gel method,[15] and is caused by the faster condensation rate of titania precursors during the solvent evaporation process. The top layer would be formed from the air interface, where the increase of the partial concentration of water by uptake of moisture and the decrease of the HCl concentration by evaporation concomitantly take place. The fast condensation at the surface leads to the rapid formation of the top layer without influence from the anisotropic substrate. The existence of the parts without alignment is also predicted by the small peak in the in-plane XRD profiles recorded when the X-rays are perpendicular to the orientation of the mesopores (Figure 1B dotted lines). On the other hand, the bottom layer would be formed relatively slow, which provides sufficient time to align by the anisotropic interactions at the substrate surface. The optimization of the coating and aging processes, including the control of the atmosphere, will lead to perfect alignment control over the entire film.

We investigated the distribution of silica in the mesoporous titania−silica composite film, because it influences the optical property of the film by changing the refractive index of the pore wall. We observed the cross-section of the film by high resolution

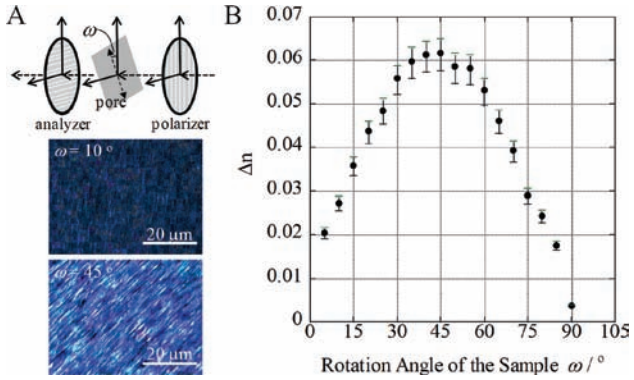

Figure 4. Characterization of the optical properties of the mesoporous titania−silica composite film with aligned mesopores. (A) Optical micrographs of the mesoporous titania−silica composite film placed between the crossed polarizers: (top) scheme of the measurement geometry, (middle) $\omega = 10°$, (bottom) $\omega = 45°$; (B) dependence of the apparent Δn value on the rotation angle ω.

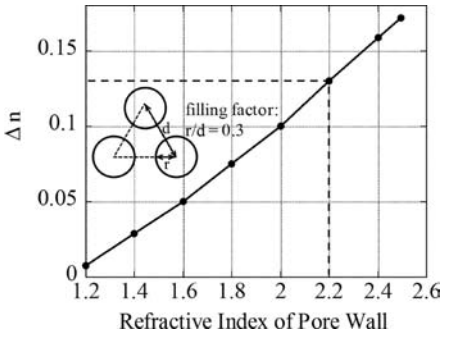

Figure 5. Calculated Δn dependence of a mesoporous film with aligned cylindrical pores on the refractive index of the pore wall, assuming the filling factor is 0.3. Inset: scheme for the definition of the filling factor.

scanning transmission electron microscopy (STEM) and measured the distributions of Ti and Si by EDX along the yellow line shown in Figure 3A. The intensity of the characteristic X-rays from Ti and Si and the output of the STEM detector, which numerically show the contrast of the image, are recorded with an interval of 1 nm. The size of the electron beam on the sample is less than 0.3 nm. The profile shown in Figure 3B clearly shows that the variation of the Ti signal is synchronized with that of the STEM contrast. On the other hand, the variation of the signal of Si is in antiphase with the above two, and the intensity is smaller at the center of the pores. This proves that the inner surface of the mesopores is coated by silica as schematically shown in Figure 3C. The Ti/Si ratio estimated by EDX is almost the same over the thickness of the film, proving that the treatment with TMOS vapor provides a uniform reinforcement with silica of the pore wall. Although the EDX does not provide a reliable atomic ratio, the result suggests the existence of considerable amount of silica that is comparable to that of titania. This indicates that at least a portion of the pore wall is a mixture of titania and silica (Figure 3C). The slight increase of the absorption around 940 cm^{-1} in the IR spectra after the TMOS vapor treatment is consistent with the formation of Ti−O−Si bonds[37] (Figure S3, Supporting Information). The titania in the mesoporous film is amorphous, which is confirmed by the absence of the diffraction peaks in the wide-angle XRD profile recorded under the parallel beam geometry (Figure S4, Supporting Information). This is due to the relatively low calcination temperature in the surfactant removal process.[29] The ordered mesoporous structure of the film is deteriorated by the increase of the calcination temperature.

Optical Properties of the Mesoporous Titania−Silica Composite Film. The prepared mesoporous titania−silica composite film shows remarkable birefringence reflecting the highly anisotropic porous structure, which results in the anisotropic apparent density. We placed this film between the crossed polarizers and observed the change of the transmittance by rotating the film. The film does not transmit light when the orientation of the mesopores is either parallel or perpendicular to the polarization of the incident light. However, the transmittance increases with the rotation of the sample, and it reaches the maximum when the rubbing direction is 45° from the polarization of the incident light. The optical micrographs of the film placed between the two polarizers, taken at $\omega = 10°$ and 45°, are shown in Figure 4A. These micrographs clearly prove the distinct birefringence of the film, and the two polarization axes are parallel and perpendicular to the rubbing direction, that is, the alignment direction of the mesopores. The optical retardation is measured as a function of the rotation angle ω (angle between the polarization of the first polarizer and the pore direction), at a wavelength of 550 nm. We estimated the apparent Δn value from the retardation data and the film thickness determined by cross-sectional SEM. As shown in Figure 4B, the estimated Δn value (at $\omega = 45°$) is larger than 0.06. Such large birefringence has never been observed in the mesoporous silica films with comparable distribution of the in-plane alignment of the mesopores, and it is undoubtedly caused by the large refractive index of titania. The birefringence in the tungsten oxide/surfactant composite film with aligned mesochannels in the plane of the film, reported by Hillhouse et al., is also much smaller than this value.[38] This is because of the existence of an organic template in the film, and our results shows the importance of a hollow structure to get high optical anisotropy.

We calculated the theoretical value of Δn by changing the refractive index of the pore wall, assuming similar porosity and a perfect uniaxial alignment, as shown in Figure 5. The filling factor of the pores at the cross-section is estimated to be ~0.3 (shown in the inset of Figure 5) from the cross-sectional STEM image, and this value is used for the calculation. The refractive index of amorphous titania films, prepared by the same procedure without adding a surfactant, is estimated to be 2.2 by ellipsometry. Assuming the refractive index of the pore wall is the same as this value, the Δn should be ~0.13, which is much larger than the present experimental result. This is mainly due to the coexistence of silica with a lower refractive index of ~1.4 in the pore walls. Preparation of an aligned mesoporous titania film without the reinforcement of silica will greatly increase the Δn value. This will be achieved by the increase of the structural period accompanied by thickening of the pore wall. The calculation teaches us that the Δn value is almost independent of the periodicity when the porosity is constant (Figure S5, Supporting Information). The existence of the top layer without in-plane alignment, which does not contribute to the optical anisotropy, also causes the underestimation of the Δn value because this is estimated by dividing the measured retardation by the total thickness of the film. Alignment control over the whole thickness is required to achieve the larger optical anisotropy. As described above, the potential Δn of the aligned mesoporous titania film is ~0.13. This Δn value is comparable with that of calcite ($\Delta n = 0.17$), a representative birefringent crystal.

The present results suggest the possibility that the in-plane alignment control of the mesopores through the anisotropic surface interactions on the rubbing-treated polyimide film can be applied for other nonsiliceous materials, whose condensation rates in aqueous medium are much faster than silica. Such anisotropic mesoporous materials with a variety in composition will find many applications in the field of optics.

CONCLUSION

We achieved the preparation of mesoporous titania−silica composite films with uniaxially aligned cylindrical pores using a rubbing-treated polyimide film as an alignment-controlling layer. The treatment of the film with TMOS vapor effectively suppresses the collapse of the structure during the calcination process. The prepared mesoporous titania−silica composite film shows a large birefringence with the Δn value over 0.06 at a wavelength of 550 nm, which is due to the large refractive index of titania that forms the pore walls and the highly anisotropic mesoporous structure. It is expected that various mesoporous films with anisotropic properties originating from the anisotropic structure will be prepared using the same method, and they will find many applications in the future.

ASSOCIATED CONTENT

Supporting Information. IR spectra of the mesostructured films, high resolution SEM images of the surface of the mesoporous titania−silica composite film, enlarged IR spectra of the mesostructured films in the 700−1000 cm^{-1} region, XRD profile of the mesoporous titania−silica composite film in a wide-angle region, calculated Δn values of the aligned mesoporous films with a filling factor of 0.3 with different lattice distances. This material is available free of charge via the Internet at http://pubs.acs.org.

AUTHOR INFORMATION

Corresponding Author
miyata.hirokatsu@canon.co.jp; kuroda@waseda.jp

ACKNOWLEDGMENT

The authors acknowledge Dr. O. Albrecht for careful review of the manuscript. The authors thank Ms. R. Ueno and Ms. A. Takai for useful advice for the experiments. Also, the authors appreciate Ms. M. Fukushima and Ms. M. Itoh for performing the preliminary experiments.

REFERENCES

(1) Hodgkinson, I. J.; Wu, Q. H. *Birefringent Thin Films and Polarizing Elements*; World Scientific Publishing Co. Pte. Ltd.: Singapore, 1997.
(2) Born, M.; Wolf, E. *Principles of Optics*; Pergamon Press: London, 1959.
(3) Yariv, A. *Optical Electronics in Modern Communications*; Oxford University Press: New York, 1997.
(4) Ogawa, M. *Chem. Commun.* **1996**, 1149–1150.
(5) Lu, Y.; Ganguli, R.; Drewien, C. A.; Anderson, M. T.; Brinker, C. J.; Gong, W.; Guo, Y.; Soyez, H.; Dunn, B.; Huang, M. H.; Zink, J. I. *Nature* **1997**, *389*, 364–368.
(6) Yang, H.; Kuperman, A.; Coombs, N.; Mamiche-Afara, S.; Ozin, G. A. *Nature* **1996**, *379*, 703–705.
(7) Aksay, I. A.; Trau, M.; Manne, S.; Honma, I.; Yao, N.; Zhou, L.; Fenter, P.; Eisenberger, P. M.; Gruner, S. M. *Science* **1996**, *273*, 892–897.
(8) (a) Yang, P.; Zhao, D.; Margolese, D. I.; Chmelka, B. F.; Stucky, G. D. *Nature* **1998**, *396*, 152–155. (b) Yang, P.; Zhao, D.; Margolese, D. I.; Chmelka, B. F.; Stucky, G. D. *Chem. Mater.* **1999**, *11*, 2813–2826.
(9) Smarsly, B.; Grosso, D.; Brezesinski, T.; Pinna, N.; Boissière, C.; Antonietti, M.; Sanchez, C. *Chem. Mater.* **2004**, *16*, 2948–2952.
(10) Grosso, D.; Cagnol, F.; Soler-Illia, G. J. A. A.; Crepaldi, E. L.; Amenitsch, H.; Brunet-Bruneau, A.; Bourgeois, A.; Sanchez, C. *Adv. Funct. Mater.* **2004**, *14*, 309–322.
(11) Sanchez, C.; Boissière, C.; Grosso, D.; Laberty, C.; Nicole, L. *Chem. Mater.* **2008**, *20*, 682–737.
(12) Innocenzi, P.; Malfatti, L.; Kidchob, T.; Falcaro, P. *Chem. Mater.* **2009**, *21*, 2555–2564.
(13) Soler-Illia, G. J. A. A.; Innocenzi, P. *Chem.—Eur. J.* **2006**, *12*, 4478–5943.
(14) (a) Miyata, H.; Kuroda, K. *J. Am. Chem. Soc.* **1999**, *121*, 7618–7624. (b) Miyata, H.; Kuroda, K. *Chem. Mater.* **2000**, *12*, 49–54. (c) Miyata, H.; Noma, T.; Watanabe, M.; Kuroda, K. *Chem. Mater.* **2002**, *14*, 766–772.
(15) (a) Miyata, H.; Kawashima, Y.; Itoh, M.; Watanabe, M. *Chem. Mater.* **2005**, *17*, 5323–5327. (b) Suzuki, T.; Kanno, Y.; Morioka, Y.; Kuroda, K. *Chem. Commun.* **2008**, 3284–3286. (c) Suzuki, T.; Miyata, H.; Kuroda, K. *J. Mater. Chem.* **2008**, *18*, 1239–1244.
(16) (a) Kawashima, Y.; Nakagawa, M.; Seki, T.; Ichimura, K. *Chem. Mater.* **2002**, *14*, 2842–2844. (b) Kawashima, Y.; Nakagawa, M.; Ichimura, K.; Seki, T. *J. Mater. Chem.* **2004**, *14*, 328–335. (c) Fukumoto, H.; Nagano, S.; Kawatsuki, N.; Seki, T. *Chem. Mater.* **2006**, *18*, 1226–1234.
(17) Yamauchi, Y.; Sawada, M.; Noma, T.; Ito, H.; Furumi, S.; Sakka, Y.; Kuroda, K. *J. Mater. Chem.* **2005**, *15*, 1137–1140.
(18) (a) Trau, M.; Yao, N.; Kim, E.; Xia, Y.; Whitesides, G. M.; Aksay, I. A. *Nature* **1997**, *390*, 674–676. (b) Hillhouse, H. W.; Okubo, T.; van Egmond, J. W.; Tsapatsis, M. *Chem. Mater.* **1997**, *9*, 1505–1507.
(19) Melosh, N. A.; Davidson, P.; Feng, P.; Pine, D. J.; Chmelka, B. F. *J. Am. Chem. Soc.* **2001**, *123*, 1240–1241.
(20) Grosso, D.; Soler-Illia, G. J. A. A.; Babonneau, F.; Sanchez, C.; Albouy, P.-A.; Brunet-Bruneau, A.; Balkenende, A. R. *Adv. Mater.* **2001**, *13*, 1085–1090.
(21) (a) Kirsch, B. L.; Richman, E. K.; Riley, A. E.; Tolbert, S. H. *J. Phys. Chem. B* **2004**, *108*, 12698–12706. (b) Richman, E. K.; Brezesinski, T.; Tolbert, S. H. *Nat. Mater.* **2008**, *7*, 712–717.
(22) Alberius, P. C.; Frindell, K. L.; Hayward, R. C.; Kramer, E. J.; Stucky, G. D.; Chmelka, B. F. *Chem. Mater.* **2002**, *14*, 3284–3294.
(23) (a) Coakley, K. M.; McGehee, M. D. *Appl. Phys. Lett.* **2003**, *83*, 3380–3382. (b) Coakley, K. M.; Liu, Y.; McGehee, M. D.; Frindell, K. L.; Stucky, G. D. *Adv. Funct. Mater.* **2003**, *13*, 301–306.
(24) (a) Bosc, F.; Ayral, A.; Alouy, P.-A.; Guizard, C. *Chem. Mater.* **2003**, *15*, 2463–2468. (b) Bosc, F.; Ayral, A.; Alouy, P.-A.; Datas, L.; Guizard, C. *Chem. Mater.* **2004**, *16*, 2208–2214.
(25) (a) Smarsly, B.; Grosso, D.; Brezesinski, T.; Pinna, N.; Boissière, C.; Antonietti, M.; Sanchez, C. *Chem. Mater.* **2004**, *16*, 2948–2952. (b) Fattakhova-Rohlfing, D.; Wark, M.; Brezesinski, T.; Smarsly, B. *Adv. Funct. Mater.* **2007**, *17*, 123–132.
(26) Choi, S. Y.; Mamak, M.; Coombs, N.; Chopra, N.; Ozin, G. A. *Adv. Funct. Mater.* **2004**, *14*, 335–344.
(27) Wu, C.-W.; Ohsuna, T.; Kuwabara, M.; Kuroda, K. *J. Am. Chem. Soc.* **2006**, *128*, 4544–4545.
(28) Crepaldi, E. L.; Soler-Illia, G. J. A. A.; Grosso, D.; Cagnol, F.; Ribot, F.; Sanchez, C. *J. Am. Chem. Soc.* **2003**, *125*, 9770–9786.
(29) Bass, J. D.; Grosso, D.; Boissiere, C.; Sanchez, C. *J. Am. Chem. Soc.* **2008**, *130*, 7882–7897.
(30) Kimura, T.; Yamauchi, Y.; Miyamoto, N. *Chem.—Eur. J.* **2010**, *16*, 12069–12073.
(31) Zhang, R.; Tu, B.; Zhao, D. *Chem.—Eur. J.* **2010**, *16*, 9977–9981.
(32) Nishiyama, N.; Tanaka, S.; Egashira, Y.; Oku, Y.; Ueyama, K. *Chem. Mater.* **2002**, *14*, 4229–4234.
(33) Katou, T.; Lee, B.; Lu, D.; Kondo, J. N.; Hara, M.; Domen, K. *Angew. Chem., Int. Ed.* **2003**, *42*, 2382–2385.

(34) Wang, K.; Morris, M. A.; Holmes, D. *Chem. Mater.* **2005**, *17*, 1269–1271.
(35) (a) Shirokura, N.; Nakajima, K.; Nakabayashi, A.; Lu, D.; Hara, M.; Domen, K.; Tatsumi, T.; Kondo, J. N. *Chem. Commun.* **2006**, 2188–2190. (b) Kondo, J. N.; Domen, K. *Chem. Mater.* **2008**, *20*, 835–847.
(36) Hisatomi, T.; Otani, M.; Nakajima, K.; Teramura, K.; Kako, Y.; Lu, D.; Takata, T.; Kondo, J. N.; Domen, K. *Chem. Mater.* **2010**, *20*, 3854–3861.
(37) Choi, K.-M.; Wakabayashi, R.; Tatsumi, T.; Yokoi, T.; Kuroda, K. *J. Colloid Interface Sci.* **2011**, *359*, 240–247.
(38) Hillhouse, H. W.; van Egmond, J. W.; Tsapatsis, M. *Langmuir* **1999**, *15*, 4544–4550.